

Influence of acidity on liquid–liquid phase transitions of mixed SOA proxy–inorganic aerosol droplets

Yueling Chen¹& Xiangyu Pei¹, Huichao Liu¹, Yikan Meng¹, Zhengning Xu¹, Fei Zhang¹, Chun Xiong¹, Thomas C. Preston³, Zhibin Wang^{1,2,4*}

¹College of Environmental and Resource Sciences, Zhejiang Provincial Key Laboratory of Organic Pollution Process and Control, Zhejiang University, Hangzhou 310058, China

²ZJU-Hangzhou Global Scientific and Technological Innovation Center, Zhejiang University, Hangzhou 311215, China

³Department of Atmospheric and Oceanic Sciences and Department of Chemistry, McGill University, 805 Sherbrooke Street West, Montreal, Quebec H3A 0B9, Canada

⁴Key Laboratory of Environment Remediation and Ecological Health, Ministry of Education, Zhejiang University, Hangzhou 310058, China

Correspondence to: Zhibin Wang (wangzhibin@zju.edu.cn)

Yueling Chen and Xiangyu Pei contribute equally to this work.

Abstract. Phase state and morphology of aerosol particles play a critical role in determining their effect on climate. While aerosol acidity has been identified as a key factor affecting the multiphase chemistry and phase transitions, the impact of acidity on phase transition of multicomponent aerosol particles has not been extensively studied in situ. In this work, we employ an aerosol optical tweezer (AOT) to probe the impact of acidity on the phase transition behavior of levitated aerosol particles. Our results reveal that higher acidity decreases the separation relative humidity (SRH) of aerosol droplets mixed with ammonium sulfate (AS) and secondary organic aerosol (SOA) proxy, such as 3-methylglutaric acid (3-MGA), 1,2,6-hexanetriol (HEXT) and 2,5-hexanediol (HEXD) across aerosol pH in atmospheric condition. Phase separation of organic acids was more sensitive to acidity compared to organic alcohols. We found the mixing relative humidity (MRH) was consistently higher than the SRH in several systems. Phase-separating systems, including 3-MGA/AS, HEXT/AS, and HEXD/AS, exhibited oxygen-to-carbon ratios (O:C) of 0.67, 0.50, and 0.33, respectively. In contrast, liquid-liquid phase separation (LLPS) did not occur in the high O:C system of glycerol/AS, which had an O:C of 1.00. Additionally, the morphology of ~~4238~~ out of the ~~460~~ aerosol particles that underwent LLPS was observed to be a core-shell. Our findings provide a comprehensive understanding of the pH-dependent LLPS in individual suspended aerosol droplets and pave the way for future research on phase separation of atmospheric aerosol particles.

1 Introduction

Atmospheric aerosol particles can directly and indirectly impact climate by absorbing and scattering light and acting as cloud condensation nuclei (Rosenfeld et al., 2014). Particle morphology is a critical factor influencing the physiochemical properties

31 of aerosols such as their optical properties, chemistry, and nucleation processes (Freedman et al., 2009; Corral Arroyo et al.,
32 2022; Cosman et al., 2008; Lam et al., 2021; Petters and Kreidenweis, 2007; Mikhailov et al., 2021). Morphology can be
33 broadly categorized into single-phase homogeneous morphology and phase separation morphology ([Bertram et al. 2011;](#)
34 [Ciobanu et al. 2009](#)~~[Gorkowski et al., 2020](#)~~), based on the phase state of the particle. For droplets with a phase separation
35 morphology, the two main equilibrium morphologies are a fully engulfed (core-shell) structure and a partially engulfed
36 structure ([Reid et al. 2011](#)~~[Freedman, 2020](#)~~). Droplets can undergo phase transition processes and thus the morphology would
37 be changed. The composition and mass of inorganic and organic components impact the phase transition characteristics of a
38 particle. With a decrease of particle water content, a transition occurs from single homogenous liquid phase to two separated
39 liquid phases, which is known as liquid-liquid phase separation (LLPS). The relative humidity (RH) when the LLPS occurs is
40 defined as separation relative humidity (SRH). The reverse process, in which two liquid phases mix into a single homogenous
41 liquid phase, is referred to as liquid-liquid phase mixing and the corresponding RH is the mixing RH (MRH; [You et al., 2014;](#)
42 [Gorkowski et al., 2017](#)).

43
44 The phenomenon of LLPS has garnered considerable attention from the atmospheric research community due to its potential
45 role in affecting the physiochemical properties of atmospheric aerosols ([Ott et al., 2020; Freedman, 2020](#)). Song et al. (2012)
46 using optical microscopy studied the relationship between LLPS and the oxygen-to-carbon ratio (O:C) and discovered that
47 LLPS was consistently observed when $O:C < 0.56$, while it was never observed when $O:C > 0.80$. For O:C between 0.56 and
48 0.80, the occurrence of LLPS was influenced by the types of organic functional groups. Gorkowski et al. (2020) utilized
49 experimental results of previous studies on LLPS and morphology, observing a general trend in morphology from partially
50 engulfed to core shell and finally homogeneous as oxidation increased. More recently, ~~[it is](#)~~[Kucinski et al. \(2021\)](#) found that
51 submicrometer-sized aerosol particles had a lower SRH compared to micrometer-sized droplets ([Kucinski et al., 2021; Ohno](#)
52 [et al., 2021](#)). Meanwhile, Stewart et al. (2015) employed aerosol optical tweezer (AOT) to investigate the morphologies of
53 aqueous droplets. They found in the polyethylene glycol (PEG)/ammonium sulfate (AS) system, droplets formed
54 predominately core-shell particles when the AS content was high and partially engulfed when the PEG content was high.

55
56 One factor that could influence the phase transitions of aerosol particles is the aerosol pH. The pH values for misty cloud and
57 fog droplets generally range between 2 and 7, whereas continental and marine aerosol particles exhibit a wider range of pH
58 values, from -1 to 5 and 0 to 8, respectively (Pye et al., 2020; Angle et al., 2021; Weber et al., 2016; Tilgner et al., 2021; Zheng
59 et al., 2020). Meanwhile, aerosol pH is size-dependent, with the fine mode showing lower 1–4 pH units than the coarse mode
60 (Fang et al., 2017; Young et al., 2013; Guo et al., 2017). [Losey et al. \(2018\) studied six organic components and discovered](#)
61 [that phase separation may be hindered by the addition of sulfuric acid, while the SRH of 3-methylglutaric acid/ammonium](#)
62 [sulfate system was found to decrease with the addition of sodium hydroxide \(Losey et al. 2016\), as the deprotonation of organic](#)
63 [component or difference in salting out ability of inorganic may change the SRH.](#)~~[Losey et al. \(2018\) measured the RH of phase](#)~~

64 ~~transitions using optical microscopy and discovered that for low-pH aerosol particles (≤ 0.35), phase separation may be~~
65 ~~hindered by the addition of sulfuric acid. However, it should be noted that the study utilized substrate-deposited droplets,~~
66 ~~which means the effect of the contact of the coverslip on droplet morphology cannot be disregarded.~~ More recently, Tong et
67 al. (2022) investigated the effect of acidity on phase separation in single suspended microdroplets using AOT. Their results
68 showed that the pH can affect the miscibility of the mixture and high acidity results in a reduced SRH of 1,2,6-hexanetriol.

69 ~~Nevertheless, parallel experiments in this study were not conducted to accurately determine the uncertainty of the~~
70 ~~measurements.~~

71 Our aim with this work is to gain a comprehensive understanding of the influence of pH on phase transitions in suspended
72 droplets. To that end, we investigate pH-dependent SRH and MRH, as well as morphologies of aqueous droplets using AOT,
73 meanwhile discussed the effect of O:C on phase separation behavior. Compared to substrate-based measurement techniques,
74 AOT can suspend droplets without any substrate contact, providing a more realistic simulation of the behavior of aerosols in
75 the atmosphere. (Wang et al., 2021; Cui et al., 2021; Redding et al., 2015; Gong et al., 2018; Rafferty et al., 2023). We measured
76 droplets containing AS and a range of organic compounds with varying O:C. We discuss how our findings provide insight into
77 the mechanisms behind pH-dependent phase transitions in levitated droplets, along with the implications for fields such as
78 climate science. Overall, our study highlights the importance of considering pH as a key factor in the phase transition behavior
79 of micron-sized droplets and underscores the need for further research to fully understand the complex interactions between
80 pH and phase transitions in these atmospherically relevant systems.

81 2 Methods

82 2.1 Aerosol generation

83 Four organics components: glycerol (GL), 3-methylglutaric acid (3-MGA), 1,2,6-hexanetriol (HEXT), and 2,5-hexanediol
84 (HEXD), were chosen because they are commonly-used secondary organic aerosol (SOA) proxies (Lam et al., 2021;
85 Gorkowski et al., 2020). O:C of the selected chemicals varied from 1 to 0.33 (**Table 1**), which is similar to the real
86 atmospheric SOA (Canagaratna et al., 2015; Mahrt et al., 2021). AS was chosen as the inorganic salt component due to its
87 widespread occurrence in the atmospheric environment. All concentrations of organics and AS in the mother solutions were
88 50 g/L. The pure organic and inorganic components were dissolved in ultrapure water (Millipore, resistivity of 18.2 M Ω) to
89 create solutions with organic-to-inorganic mass ratio (OIR) of 1:1. The pH of studied system were adjusted within the range
90 of 0.48 to 6.53 by~~The pH of each solution was measured using a pH meter (Mettler Toledo Instruments Co., Ltd., Shanghai,~~
91 ~~China), and adjusted as necessary~~ using either concentrated sulfuric acid (SA) or sodium hydroxide (NaOH) solution (5.29
92 mol/L). Sodium hydroxide, a strong base, allowed for pH adjustment with minimal usage (Losey et al., 2016). However, it is
93 necessary to acknowledge that the addition of NaOH changes the composition of the inorganic part of the solution, potentially
94 affecting the SRH values measured. For the 3-MGA/AS system, either SA or NaOH was utilized, while for the HEXT/AS and

95 [HEXD/AS systems, only SA was used. The pH of each solution was measured using a pH meter \(Mettler Toledo Instruments](#)
96 [Co., Ltd., Shanghai, China\).](#) ~~Four to six solutions were prepared for each system with pH values ranging from 0.48 to 6.53.~~ The
97 purity and supplier of the compounds used in this study were summarized in **Table S1**.

98 **Table 1.** Information of the solutions used to generate aerosol droplets.

Solution ID	Organic component	O:C ratio	pH
GL	glycerol	1.00	5.24±0.01
3-MGA-I	3-methylglutaric acid	0.67	0.48±0.01
3-MGA-II			1.19±0.01
3-MGA-III			2.70±0.01
3-MGA-IV			3.70±0.01
3-MGA-V			5.21±0.02
3-MGA-VI			6.53±0.02
HEXT-I	1,2,6-hexanetriol	0.50	0.92±0.01
HEXT-II			2.02±0.01
HEXT-III			3.14±0.01
HEXT-IV			5.11±0.02
HEXD-I	2,5-hexanediol	0.33	1.39±0.01
HEXD-II			2.03±0.01
HEXD-III			2.71±0.01
HEXD-IV			3.13±0.01
HEXD-V			5.01±0.01

99

100 2.2 Experimental setup

101 A schematic illustration of the experimental setup is presented in **Fig. S1**. The aerosol optical tweezer system consists of a
102 custom-made levitation chamber that integrates the optical trapping system, the illumination and imaging system, and the
103 aerosol generation system. A 532 nm (Opus 532-2W) laser was used to create an optical trap with a 100x oil immersion
104 objective (Olympus, UPLFLN100XO, NA 1.30) pressed against a glass coverslip (Nest, thickness 160-190 μm). The
105 illumination and imaging system includes a 450 nm LED (Daheng Optics, GCI060404) and a camera (Thorlabs, CS165CU/M)
106 to illuminate and image the particle. Two low pass filters (Andover, 500FL07-25) were used in front of the camera lens to
107 remove the influence of back scattered light of the 532 nm laser to photograph clear image of the particle. The Raman scattered
108 light passed through two 50:50 beam splitters (CVI Laser Optics, BTF-VIS-50-2501M-C) and a notch filter (Semrock, NFD01-
109 532-25x36) and was focused into the Raman spectrograph. A spectrograph (ZOLIX, Omni-λ5004i) is used to measure the

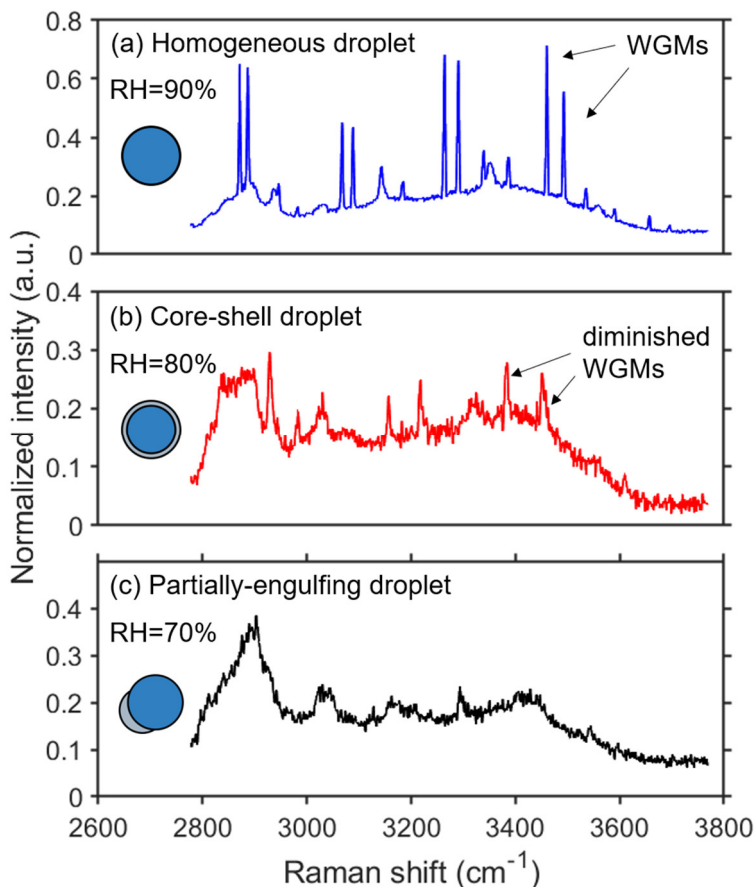
110 Stokes shifted Raman spectrum. A 20 μm entrance slit width and 1200 groove/mm diffraction grating with blaze wavelength
111 of 500 nm were used to achieve a spectral resolution of 0.021 nm. The wavelength position of spectrograph was calibrated
112 with Hg-laser. The Raman scattered light was recorded every 4 second with range of 624.24-665.40 nm.

113
114 As droplets are introduced continuously into the chamber from a medical nebulizer (LANDWIND, PN100), smaller droplets
115 undergo a process of collision and coalescence, leading to the formation of larger droplets that can be readily trapped near the
116 focal point of the laser. In most cases, droplets can be successfully captured within 30 s after the introduction of an aerosol
117 plume into the cell. Air with relative humidity (RH) of 100% and 0% were mixed to produce wet air with a desired RH. The
118 flow rates of the humidified and dry air streams were regulated by mass flow controllers (MFCs, Tianjin Gastool Instruments
119 Co., Ltd., Tianjin, China, GT130D), with a combined flow rate of 0.3 L/min in total. Two humidity sensors (Sensirion, SHT85)
120 were utilized, with a precision of $\pm 1.5\%$. Since the sensor located behind the chamber was positioned in close proximity (~ 80
121 mm) to the droplet, its observed values were used as a surrogate for measuring the RH inside the chamber. The RH values
122 were reduced in increments of 5% every 30 minutes (Tong et al., 2022; Stewart et al., 2015) until droplet phase separation
123 occurred. The measured values of RH given by the sensors were used as the phase separation RH. Subsequently, the RH level
124 was set to 100%, to investigate the phase mixing of the droplets. The entire experiment was repeated $\pm 2 \sim 4$ times for each
125 system.

126 2.3 Determination of phase transitions

127 When a transparent or weakly absorbing spherical particle is trapped, it can behave as a high-quality factor optical cavity that
128 supports sharp optical resonances, resulting in cavity-enhanced Raman scattering. These resonances can be observed as peaks
129 in the Raman spectrum of a particle and are often referred to as whispering gallery modes (WGMs). In principle, particle
130 morphology can be deduced from the WGMs, as inhomogeneities in the refractive index can disrupt the circulation of the
131 WGMs (Lin et al., 1992; Mitchem et al., 2006). Raman spectra measurements of single droplets in various morphological
132 states are presented in **Figure 1**. When the droplet was in a homogeneous phase morphology, the droplet acted as a high-
133 quality microcavity and sharp WGM peaks overlapped with the spontaneous Raman spectrum (**Fig. 1a**). When the droplet was
134 in a state of a core-shell structure, observed WGMs were clearly diminished in measured spectra (**Fig. 1b**). The origin of the
135 damping of the WGMs is the radial homogeneity that is present when the particle is separated into a hydrophilic core and a
136 hydrophobic shell. As a result, when fitting the Raman spectra with the Mie scattering model for homogeneous droplets, the
137 error in the best-fits greatly increase. Examination of the retrieved radius and refractive index reveals a clear break with fits
138 for that of a homogeneous sphere. Therefore, the point at which a significant break in particle size and refractive index occurred
139 can be used as the point at which core-shell phase separation occurs. As illustrated in **Fig. 1c**, when the droplet was partially-
140 engulfed and non-spherical, WGM peaks in the spectrum are absent (Reid et al., 2011). The origin of the spontaneous Raman
141 peaks at 3300 cm^{-1} and $\sim 3050\text{ cm}^{-1}$ are identified as the spurious or weakened WGM peaks and the vibration of N-H bond,

142 respectively. Overall, the results of this analysis demonstrate the dynamic changes in the Raman spectra of single droplets as
143 they undergo morphological transitions (Sullivan et al., 2020; Stewart et al., 2015; Tong et al., 2022).



144
145 **Figure 1.** Raman spectra of 3-MGA-II microdroplets: (a) a homogenous droplet (RH = 90%); (b) a core-shell droplet (RH =
146 80%); (c) a partially-engulfed droplet (RH=70%). The WGMs are marked by black arrows. The normalization of the peak is
147 achieved by dividing it by the maximum value of the spectrum's intensity, respectively.
148

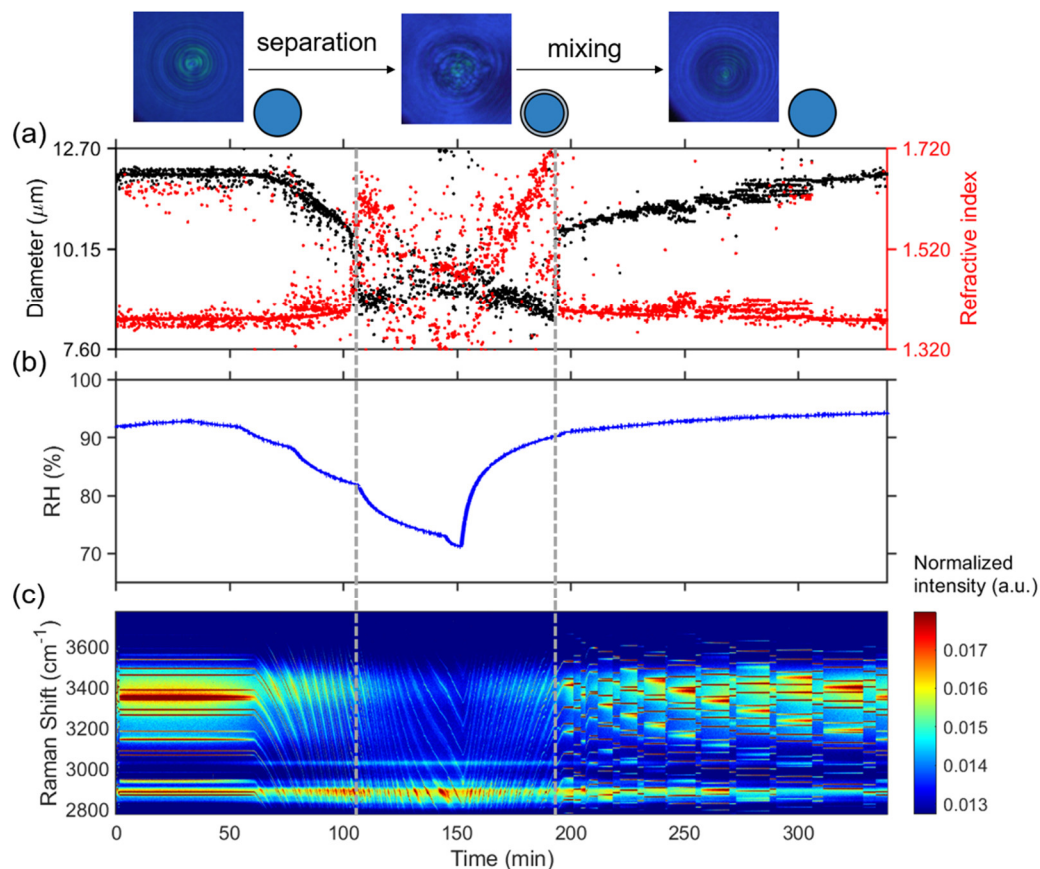
149 The peak finding method used in this study is based on the ipeak code developed by O'Haver (2022). In short, the code first
150 smooths the first derivative of the signal and identified downward-going zero-crossings that met a certain predetermined
151 minimum slope and amplitude threshold. By adjusting the corresponding parameters, it is possible to accurately detect the
152 desired peaks. The algorithm used to fit WGM peaks in spectra from homogenous spheres in this study was proposed by
153 Preston and Reid (2013) and Preston and Reid (2015). The algorithm compares observed peak positions to expected positions
154 calculated using a resonance condition from Mie theory. Error is minimized by varying particle size and refractive index (i.e.
155 the parameters of best-fit). The method has been demonstrated to provide a rapid determination of the fitted radius and

156 refractive index with an accuracy of ± 2 nm and ± 0.0005 , respectively. ~~All of the Raman spectra used in this study were~~
157 ~~normalized by the area below the spontaneous Raman signals.~~ During the experiment with reduced RH, we had to adjust the
158 ~~laser power to ensure the stable capture of droplets, which will affect the peak intensity. To eliminate this effect, as~~
159 ~~demonstrated by Tong et al. (2022), we normalized all Raman spectra used in this study by the area below the spontaneous~~
160 ~~Raman signals.~~
161

162 3 Results and discussion

163 3.1 Phase behaviors of droplets mixed SOA proxy with AS

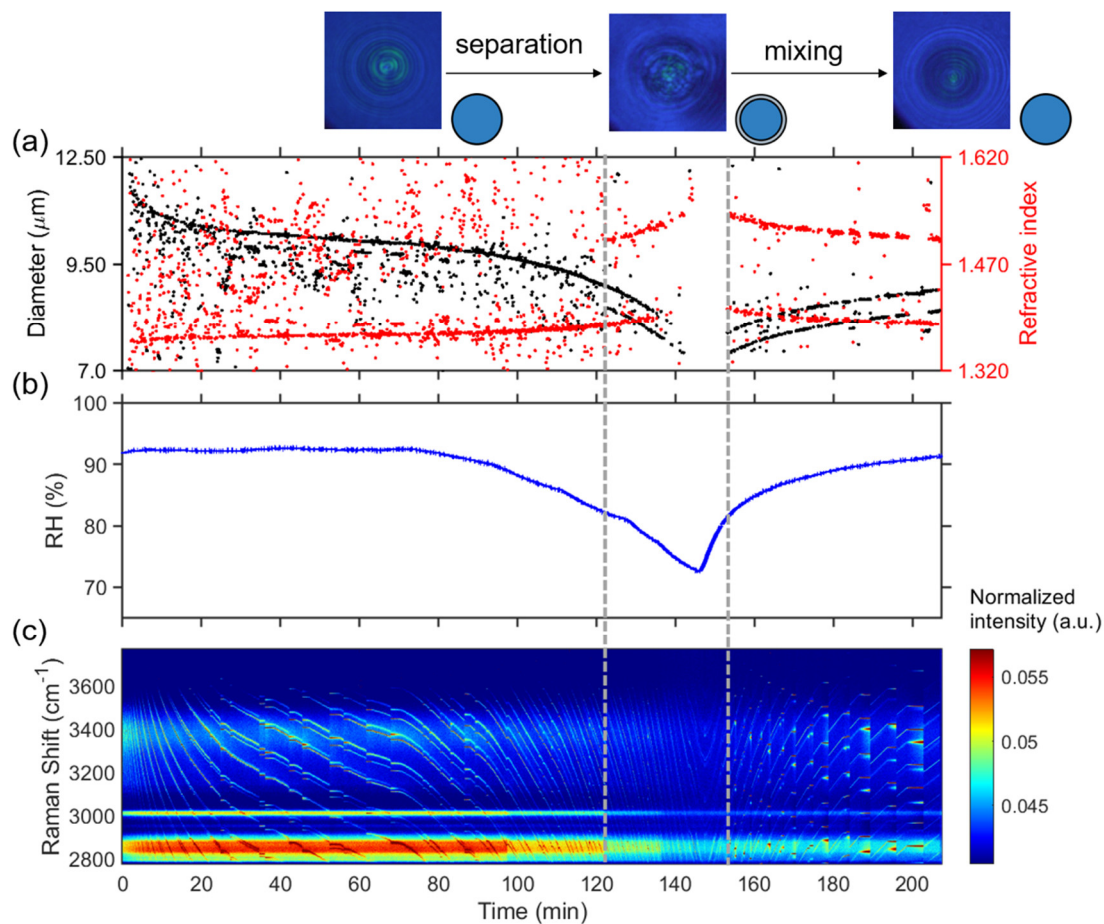
164 **Fig. 2** presents the results of time-resolved Raman spectra of aerosol droplets produced from a 3-MGA-II solution under
165 continuously varying RH, as well as the corresponding particle size and refractive index values. To enable temperature and
166 RH to stabilize, the chamber was conditioned with airflow for 50 minutes after trapping a particle. During the dehumidification
167 process, the particle diameter decreased from 11.85 μm to 9.03 μm and the refractive index increased from 1.379 to 1.475
168 when RH decreased from 93.0% to 70.0%. The particle size and water content decreased with RH due to the equilibrium
169 partitioning of water molecules between vapor and droplets. Meanwhile, the refractive index of the droplets gradually increased
170 as the water content decreases. When LLPS occurred, the droplets changed from a symmetrical homogeneous phase to either
171 an asymmetrical partially engulfed structure which led to the disappearance of the WGMs, or the formation of a core-shell
172 structure. As RH in the reaction chamber was reduced, the LLPS was initiated, marked by the variations of the WGM signal
173 (See **Fig. 1b**). This was achieved by reducing setting RH (setting values) by 5% at 30-minute intervals until the organic phase
174 separated from the water-rich phase and then continuing decreasing RH by 10%-15%. **Fig. 2a** illustrates how the fitting of the
175 droplet diameter and the refractive index deteriorated as the shell develops, indicating phase separation. The refractive index's
176 shift results from a significant change in the radial profile due to the formation of a core-shell structure. Additionally, the
177 persistence of strong WGMs indicates that the morphology of the droplet remains spherical following LLPS and is core-shell.
178 During the RH increased from 70% to 95%, the reappearance of the continuously shifting WGM signal is observed, suggesting
179 that the inorganic phase has mixed with the organic phase, and droplet returned to a homogeneous phase. During the
180 humidification process, there is an opposite trend observed in the particle size and refractive index of the droplet compared to
181 the dehumidification process. In conclusion, the variations of the WGM signal can serve as a reliable indicator of the
182 occurrence of liquid-liquid phase separation or mixing, and the RH at these points can be considered as the SRH or MRH,
183 respectively. The observed phase transitions of droplets produced from HEXT-IV and HEXD-V solutions were shown in **Fig.**
184 **S2-3** and **Fig. S3-4** respectively.
185



186

187 **Figure 2.** Liquid-liquid phase separation and mixing of aqueous 3-MGA-II. Schematic diagram of phase states is on the top
 188 of the figure. (a) Timescale of changes in droplet size and refractive index, determined from fitting the Raman shift positions
 189 of the WGMs. (b) RH variation after the trapping chamber during the humidity changing process. (c) Time-resolved Raman
 190 spectra. The cessation of the random motion of inclusions within the droplet and the resultant formation of a core-shell
 191 structure are indicated by the grey dashed line on the left. The grey dashed line on the right serves as an indication of the point at which
 192 the droplet morphology transitioned from a state of separated phases to a homogeneous phase. The Raman spectra at 53 min, 113
 193 min, 130 min are shown in **Fig. 1(a), (b), (c)**, respectively. Fitting errors of the WGMs were presented in **Fig. S35**.

194



195
 196 **Figure 3.** Liquid-liquid phase separation of aqueous of HEXT-IV. (a) Timescale of changes in droplet size and refractive index,
 197 determined from fitting the Raman shift positions of the WGMs. (b) RH variation after the trapping chamber during the
 198 humidity changing process with time. (c) Time-resolved Raman spectra. The cessation of the random motion of inclusions
 199 within the droplet and the resultant formation of a core-shell structure are indicated by the grey dashed line on the left. The
 200 grey dashed line on the right serves as an indication of the point at which the droplet morphology transitions from a state of
 201 phase separation to a homogeneous phase morphology. This transformation is characterized by the occurrence of phase mixing.
 202

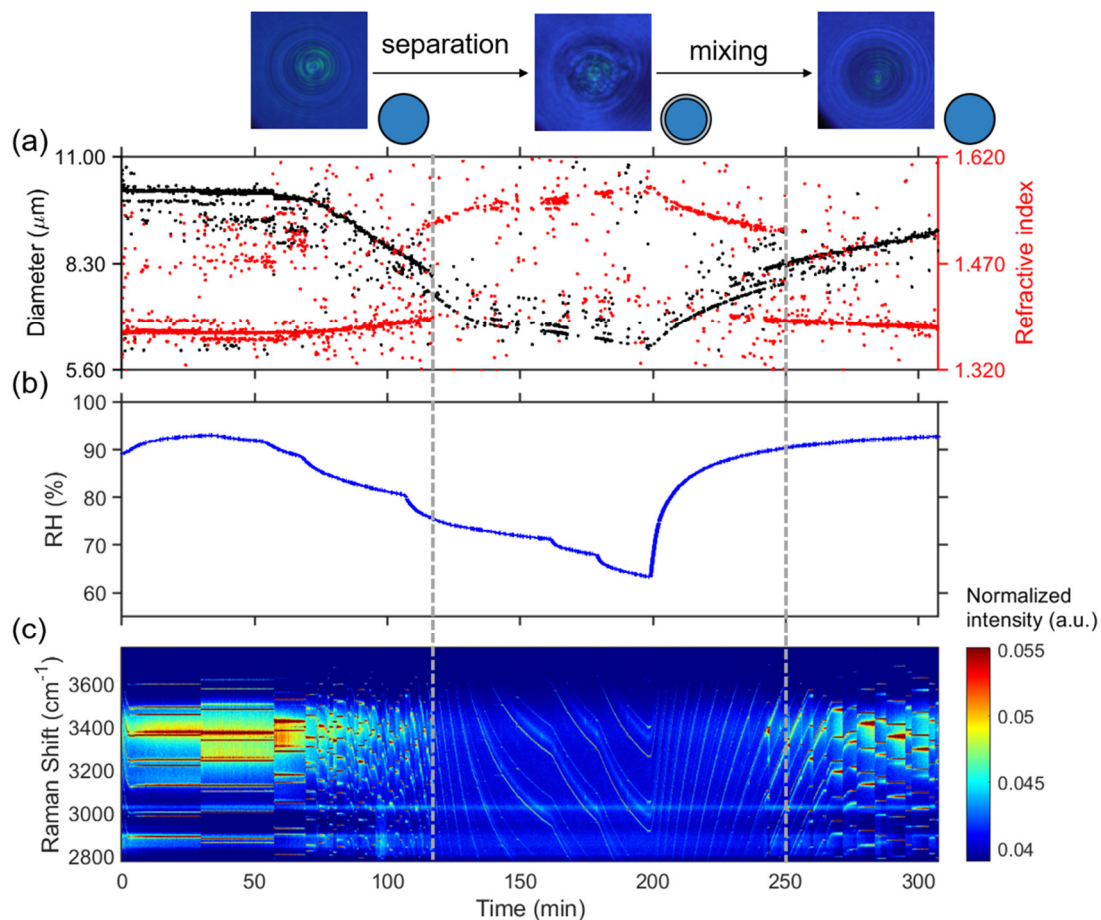


Figure 4. Liquid-liquid phase separation of aqueous of HEXD-V. (a) Timescale of changes in droplet size and refractive index, determined from fitting the Raman shift positions of the WGMs. (b) RH variation after the trapping chamber during the humidity changing process. (c) Time-resolved Raman spectra. The cessation of the random motion of inclusions within the droplet and the resultant formation of a core-shell structure are indicated by the grey dashed line on the left. The grey dashed line on the right serves as an indication of the point at which the droplet morphology transitions from a state of phase separation to a homogeneous phase morphology. This transformation is characterized by the occurrence of phase mixing.

Figure S2 presents the results of time-resolved Raman spectra of aerosol droplets produced from GL/AS solution under continuously varying RH, as well as the corresponding particle diameter and refractive index values. At the start of the experiment, the chamber RH was held at 93% for approximately 75 minutes. The spectrum during this period reveals a clear bright trend, indicative of the presence of many WGMs in the newly captured droplets. As the chamber RH dropped to a minimum value of 71.5% at around 200 minutes, the position of the WGMs in each spectral snapshot shifted continuously, following the same trend as the chamber RH. This observation suggests that the droplet was homogeneous and that no phase

217 separation occurred in the experimental RH range. The phenomenon regarding the GL/AS system is consistent with the
218 conclusion by Song et al. (2013) and Gorkowski et al. (2020).

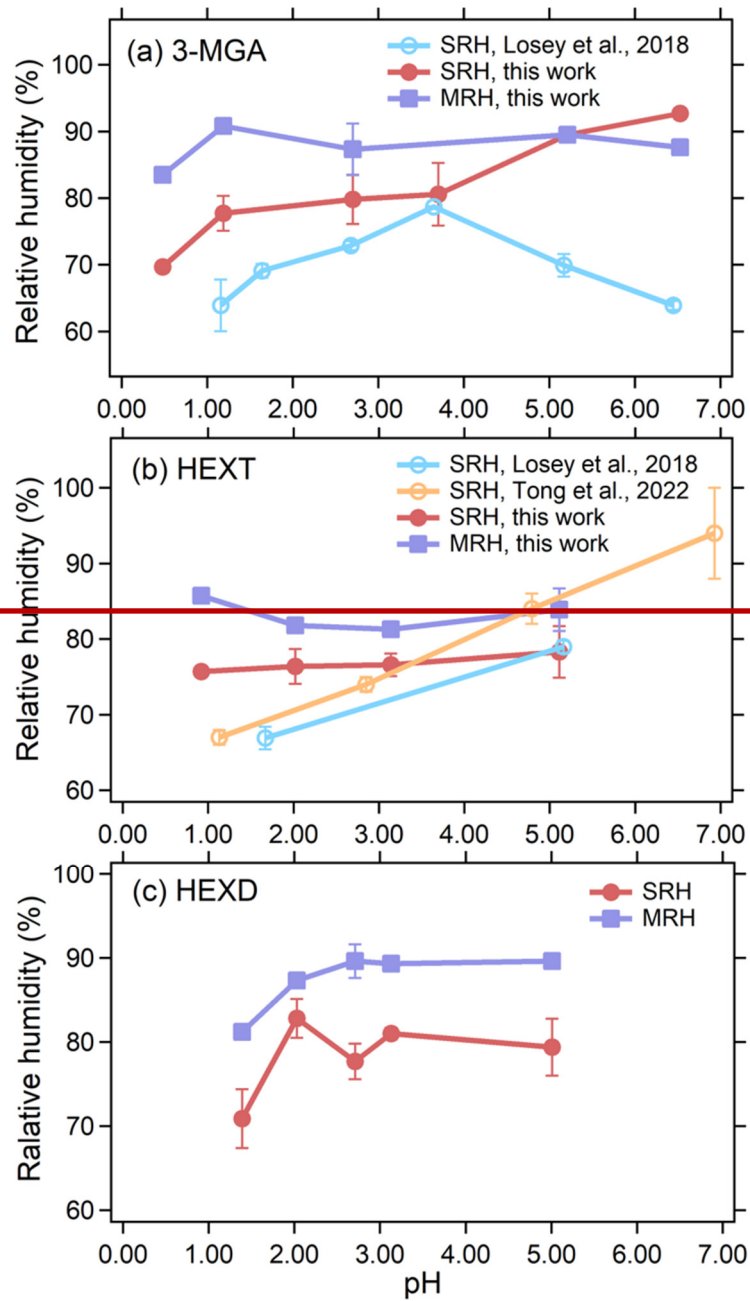
219 3.2 Effect of pH on SRH and MRH of different systems

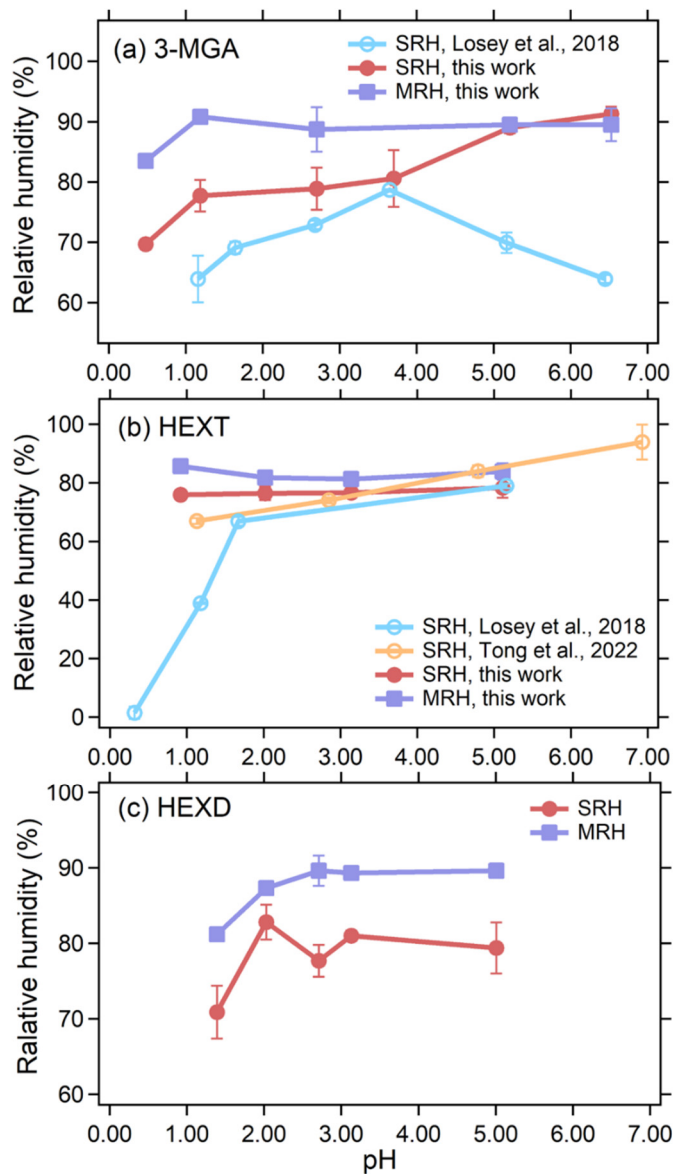
220 The SRH and MRH of aerosol droplets produced from 3-MGA-I~VI solution are shown in Fig. 53a and Table S2. The SRH
221 values were 92.7%, 89.5%, 80.6%, 79.7%, 76.2% and 69.7% at pH of 6.53, 5.21, 3.70, 2.70, 1.19 and 0.48, respectively. It is
222 worth mentioning that when the pH of the 3-MGA system is 0.48, only two sets of valid parallel experimental data are available,
223 even though we had repeated the experiment several times. Because in other parallel experiments, the SRH of the droplet is
224 lower than the capture range of AOT, the AOT would not be able to continue the capture when the particle size decreases to
225 ~6 μm. Therefore, the actual SRH may be a bit lower at this pH, but this does not affect the results we discuss later. With a
226 decrease in pH, ammonium sulfate transforms into ammonium bisulfate. Predicted by the Hofmeister series, ammonium
227 bisulfate exhibits a weaker salting out effect compared to ammonium sulfate and This decrease in SRH was attributed to the
228 salting out ability of ammonium sulfate that is weakened at lower pH, and thus hinders the ability of organic matter to
229 precipitate out of the solution (Losey et al., 2018). The MRH values at pH 6.53, 5.21, 2.70, 1.19 and 0.48 were 87.6%, 89.5%,
230 87.3%, 83.9% and 83.5%, respectively, and are generally higher than corresponding SRH, especially in the low pH range
231 (<5.00). The hysteresis between SRH and MRH existed because the SRH process has an activation barrier while the MRH
232 process does not, and lower RH is needed for the aerosol droplet to overcome the activation barrier to form two phases
233 (Freedman, 2020). Similar results were also observed in HEXT/AS and HEXD/AS systems. Additionally, the pH-dependent
234 SRHs obtained in this study were compared to those reported by Losey et al. (2018), as depicted in Fig. 53a. It is worth
235 mentioned that the solute concentration used in our study (50g/L) is comparable to Losey et al. (2018) (5.0 wt%), allowing for
236 meaningful comparison of results. Overall, the SRHs of 3-MGA obtained in this study was higher than the results of Losey et
237 al. (2018). When the pH was lower than 3.70, in 3-MGA system, the present study followed a similar trend as the results of
238 Losey et al. (2018), with the SRH decreasing as the pH decreased. However, when the pH was greater than 3.70, our study
239 showed an opposite trend compared to the results of Losey et al. (2018). The observed discrepancy may be attributed to the
240 distinct ambient conditions of the droplets, different methodologies employed. The laser levitation, resulting in a spherical
241 morphology, while the optical microscopy involves substrate deposition, leading to a morphology resembling a spherical
242 crown (Tong et al., 2022; Zhou et al., 2014) The present study utilized an optical tweezer system to capture droplets of ~10 μm
243 diameter and the results were obtained using a spectrometer, while Losey et al. (2018) allowed ~100 μm size droplets to settle
244 on a hydrophobic surface and observed the samples using an optical microscope. Kucinski et al. (2019) reported that the
245 particle size has a significant impact on the phase separation of micro-droplets. The spherical morphology and smaller size in
246 this study enhances the Kelvin effect, resulting in higher possibilities of phase separation occurring within droplets. The
247 difference in droplet size is significant and the droplets used in this study are more representative of real atmospheric particulate
248 matter, whereas the droplet properties in Losey et al. (2018) may be influenced by the surface they came into contact with.

249 ~~The underlying reasons for these differences are currently unclear, and further investigations are needed. Thus, the utilization~~
250 ~~of an optical tweezer system provides a more realistic simulation of the evolution of particulate matter in the atmosphere.~~

251
252 In addition to 3-MGA, we also studied two organic/AS systems to investigate how acidity affects SRH and MRH of aerosols
253 of differing composition. These results are shown in **Fig. 53** and tabulated in **Table 2**. The separation diameter (SD) of 3-
254 MGA/AS ranges from 7.23 μ m to 9.74 μ m, with a corresponding separation refractive index (SRI) ranging from 1.362 to 1.515.
255 For HEXT/AS, the SD ranges from 9.01 μ m to 9.90 μ m, while the SRI ranges from 1.396 to 1.421. Lastly, the SD of HEXD/AS
256 ranges from 7.45 μ m to 8.97 μ m, with the SRI ranging from 1.382 to 1.406. The data suggests that acidity did not have a
257 noticeable effect on the MRH of the various systems. The pH of the HEXT/AS solution without the addition of any acid was
258 5.11, and sulfuric acid was utilized to adjust the pH to lower levels (3.14, 2.02 and 0.92). The SRH values of HEXT/AS system
259 (O:C=0.50) decreased as the pH decreased, with values of 78.3%, 76.6%, 76.4% and 75.7% at pH values of 5.11, 3.14, 2.02
260 and 0.92, respectively. The trend is similar to the 3-MGA (O:C=0.67) system, and the reason why SRH decreased may be due
261 to the acid enhancing the miscibility of organic alcohols and inorganic substances, resulting in a greater difficulty in separating
262 the hydrophobic phase from the water-rich phase (Tong et al., 2022). Still, we observed SRH was not strongly dependent on
263 pH for HEXT/AS, compared to 3-MGA/AS system. This is likely due to the fact that organic alcohols have a large pK_a (e.g.
264 the pK_a of HEXT is 14.3) and therefore exhibit minimal ionization in the pH range studied here (Wade and Simek, 2020).
265 Additionally, the relative molecular interactions between alcohols and water are weaker than those of acids, leading to a weaker
266 dependence of salting out ability of AS in the HEXT/AS system. The results of Losey et al. (2018) and Tong et al. (2022) were
267 also depicted in **Fig. 53b**. Our results ~~differ from~~ ~~were higher than~~ those of Losey et al. (2018), ~~who observed a significant~~
268 ~~decline in SRH as the pH decreased~~ ~~but the trend was similar~~. ~~The specific reason for the discrepancy remains unclear, but we~~
269 ~~speculate it may due to different condition of droplet~~ ~~We attribute this discrepancy to a similar reason as that of the 3 MGA/AS~~
270 ~~system, which was previously discussed in this article~~. ~~Moreover, the concentration of HEXT in this work (50g/L) is higher~~
271 ~~than concentration (2.5 wt%, about 26 g/L) of Losey et al. (2018)~~. ~~The higher concentration may enhance the precipitation of~~
272 ~~organic matter from the inorganic salts in our work~~. In contrast to the findings of Tong et al. (2022), our study observed a less
273 pronounced trend in the values of SRH, and a narrower range in the distribution of SRH compared to literature values. The
274 difference in OIR between this study (1:1) and Tong et al. (2022) (2:1) may account for the discrepancy in SRH. Previous
275 studies (Ma et al., 2021; Stewart et al., 2015; Song et al., 2012) indicated that OIR differences could affect SRH, but SRH was
276 not significantly dependent on OIR. The discrepancy in SRH may also be due to the variations in experimental conditions,
277 such as laser power, experimental duration, etc. For HEXD/AS (O:C=0.33) system, SRH decreases significantly when the pH
278 is less than 2.00, while acidity had no significant effect on SRH when pH is greater than 2.00, with values of 79.4%, 81.0%,
279 77.7%, 82.8% and 70.9% at pH values of 5.01, 3.13, 2.71, 2.03 and 1.39, respectively. This phenomenon was attributed to a
280 mechanism similar to that observed in HEXT/AS. To our knowledge, this is the first investigation on the pH-dependent phase
281 transition of HEXD/AS at the single particle level in a contact-free environment.

283 The pH values of misty cloud and fog droplets typically fall within the range of 2 to 7, whereas continental and marine aerosol
284 particles display a broader spectrum of pH values (Pye et al., 2020; Tilgner et al., 2021). Our research suggests that in real
285 atmospheric conditions where many ambient aerosol particles exhibit high acidity (Angle et al., 2021; Song et al., 2018; Liu
286 et al., 2019; Li et al., 2022), phase separation behavior of droplets may be influenced significantly by droplets encounter
287 heightened impediments to phase separation and tend to display a homogeneous structure their acidity. It is challenging to
288 measure the droplet pH of the investigated system using AOT. Although we used bulk solution pH as an indicator of pH at
289 droplet phase transition. However, previous studies (Craig et al., 2018; Coddens et al., 2019; Li et al., 2023) have shown that at
290 high RH (90%~100%), the difference in the pH values between droplets and bulk solution is relatively small the pH deviation
291 between single microdroplet measurements and bulk solution measurements is small. Therefore, we used bulk solution pH as
292 an indicator of pH at droplet phase transition we consider our results valid. However, this study focused on volatile organics
293 and was conducted over a relatively long period, which may have affected our results. Nevertheless, the organic compounds
294 used in this study have low volatility. For instance, the vapor pressure of 3-MGA is 7.41×10^{-7} to 2.92×10^{-4} mmHg
295 (DTXSID50871000, United States Environmental Protection Agency), compare to normal volatile organic components of
296 atmospheric aerosol, such as 2-Methyl-1-propanol with vapor pressure of 10.5 to 16.4 mmHg (DTXSID0021759, United States
297 Environmental Protection Agency). Volatility information of other organics are provided in the Table S5. Also, the influence
298 of droplet size change in our system can be neglected since the droplets studied here were relatively large (diameter 6–14 μm),
299 we believe that any such influence can be neglected. For example, as shown in Fig. 2, the droplet size is basically same at the
300 beginning and the end of the experiment at the same RH 93.0% (11.85 μm at the beginning and 11.79 μm at the end).





303
 304 **Figure 53.** SRHs and MRHs as a function of pH for (a) 3-MGA/AS system, (b) HEXT/AS system, (c) HEXD/AS system.
 305 Hollow circles represent data from Losey et al. (2018) and Tong et al. (2022). The error bars of SRHs and MRHs are derived
 306 from multiple measurements.
 307

Table 2. SRH information for each pH studied as well as initial diameter, separation diameter (SD), separation refractive index (SRI), MRH, mixing diameter (MD), and mixing refractive index (MRI) data.

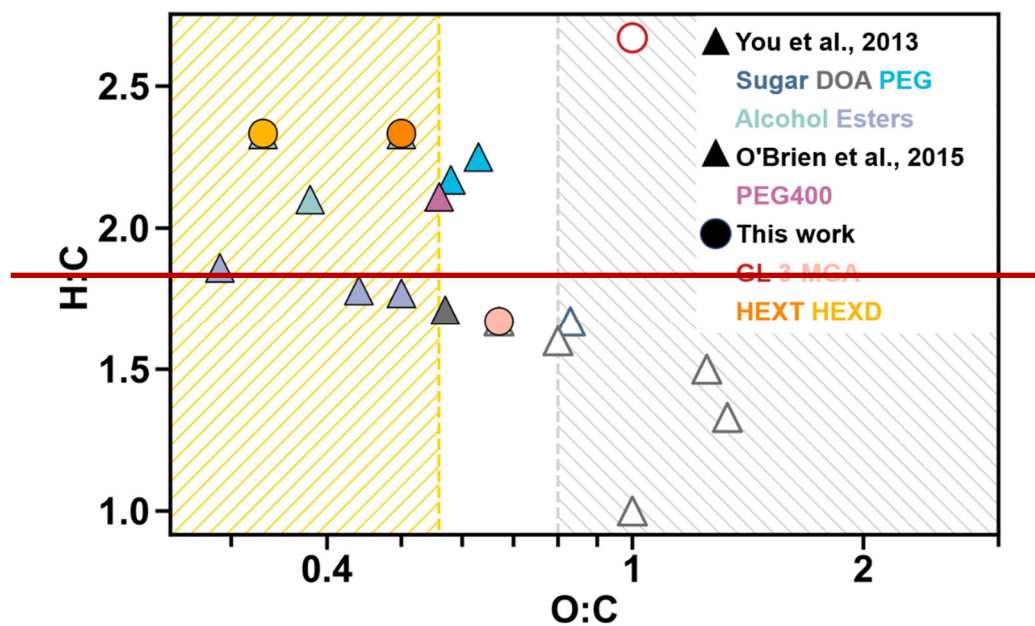
3-MGA/AS system (O:C=0.67)							
Initial pH	Initial Diameter(nm)	SRH (%)	SD (nm)	SRI ($\lambda=650\text{nm}$)	MRH (%)	MD (nm)	MRI ($\lambda=650\text{nm}$)
0.48	10.97±1.57	69.7±0.2	7.23±1.72	1.515±0.086	83.5	6.82	1.540
1.19	11.23±1.20	77.7±2.6	8.68±2.38	1.454±0.100	90.8±0.2	9.08±1.64	1.394±0.009
2.70	10.60±2.28	79.8±3.7	7.83±1.71	1.480±0.112	87.3±3.9	7.86±1.63	1.483±0.118
3.70	10.87±1.87	80.6±4.7	7.24±1.00	1.491±0.088			
5.21	11.65±1.80	89.5±0.4	8.88±0.20	1.369±0.007	89.5	7.89	1.381
6.53	13.79	92.7	10.10	1.262	87.6	7.85	1.387
HEXT/AS system (O:C=0.50)							
0.92	14.04	75.7	10.58	1.438	85.7	10.83	1.420
2.02	12.88±1.0	76.4±2.3	9.09±0.46	1.409±0.007	81.8	9.34	1.410
3.14	12.31±0.8	76.6±1.5	9.01±0.47	1.408±0.002	81.3	9.04	1.409
5.11	13.53±0.4	78.3±3.4	9.15±0.35	1.396±0.014	83.9±2.8	9.04±0.73	1.412
HEXD/AS system (O:C=0.33)							
1.39	11.48±0.78	70.9±3.5	7.45±0.77	1.406±0.008	81.2	7.93	1.406
2.03	10.54±0.57	82.8±2.3	7.90±0.99	1.382±0.007	87.3	8.83	1.392
2.71	14.55±1.36	77.7±2.1	8.30±0.28	1.391±0.009	89.6±2.0	8.53±0.32	1.388±0.010
3.13	11.02±0.62	81.0±0.7	8.97±0.22	1.384±0.016	89.3	9.14	1.384
5.01	12.22±2.73	79.4±3.4	8.33±0.40	1.384±0.019	89.6±0.1	8.38±0.54	1.390±0.004
3-MGA/AS system (O:C=0.67)							
Initial pH	Initial Diameter(μm)	SRH (%)	SD (μm)	SRI ($\lambda=650\text{ nm}$)	MRH (%)	MD (μm)	MRI ($\lambda=650\text{ nm}$)
0.48	10.97±1.57	69.7±0.2	7.23±1.72	1.515±0.086	83.5	6.82	1.540
1.19	11.23±1.20	77.7±2.6	8.68±2.38	1.454±0.100	90.8±0.2	9.08±1.64	1.394±0.009
2.70	12.02±2.94	78.9±3.5	7.88±1.21	1.493±0.082	88.7±3.7	6.81±2.76	1.506±0.094
3.70	10.87±1.87	80.6±4.7	7.24±1.00	1.491±0.088			
5.21	11.06±1.63	89.0±0.9	8.93±0.16	1.362±0.014	89.5	7.89	1.381
6.53	13.73±0.41	91.3±1.2	9.74±0.36	1.444±0.187	89.5±2.7	7.89±0.06	1.383±0.01
HEXT/AS system (O:C=0.50)							
0.92	13.52±1.6	75.9±0.2	9.90±0.76	1.421±0.017	85.7	10.83	1.420
2.02	12.88±1.0	76.4±2.3	9.09±0.46	1.409±0.007	81.8	9.34	1.410
3.14	12.31±0.8	76.6±1.5	9.01±0.47	1.408±0.002	81.3	9.04	1.409
5.11	13.53±0.4	78.3±3.4	9.15±0.35	1.396±0.014	83.9±2.8	9.04±0.73	1.412
HEXD/AS system (O:C=0.33)							
1.39	11.48±0.78	70.9±3.5	7.45±0.77	1.406±0.008	81.2	7.93	1.406
2.03	10.54±0.57	82.8±2.3	7.90±0.99	1.382±0.007	87.3	8.83	1.392
2.71	14.55±1.36	77.7±2.1	8.30±0.28	1.391±0.009	89.6±2.0	8.53±0.32	1.388±0.010

<u>3.13</u>	<u>11.02±0.62</u>	<u>81.0±0.7</u>	<u>8.97±0.22</u>	<u>1.384±0.016</u>	<u>89.3</u>	<u>9.14</u>	<u>1.384</u>
<u>5.01</u>	<u>12.22±2.73</u>	<u>79.4±3.4</u>	<u>8.33±0.40</u>	<u>1.384±0.019</u>	<u>89.6±0.1</u>	<u>8.38±0.54</u>	<u>1.390±0.004</u>

3.3 Effect of O:C on phase separation behavior in different systems

Our findings provide evidence that phase separation of droplets persists even when the organic-inorganic system is adjusted to a specific level of acidity. An important determinant of whether droplets undergo phase separation is the O:C. To illustrate this, we have included a plot in Fig. S4, which show cases the experimental system used in our study alongside relevant literature values.~~The phase separation behavior of organic aerosol particles is strongly influenced by their O:C. One point that needs to be declared is Fig. S4 only plotted for systems with no additional H₂SO₄ or NaOH.~~ As shown in Fig. S44, our findings, as well as those from previous studies (You et al., 2013; O'Brien et al., 2015), indicated that there is no correlation between the occurrence of LLPS and the hydrogen-to-carbon (H:C) ratios of the organics, which is consistent with results in previous findings (Bertram et al., 2011; Song et al., 2012). However, a clear trend was observed between LLPS occurrence and the O:C of the organic components. We observed that droplets of 3-MGA/AS, HEXT/AS and HEXD/AS systems with O:C between 0.33 and 0.67 undergo LLPS. With the decrease of water content in the droplets, two distinct phases were formed: an organic-rich phase and a salt-rich aqueous phase, under both acidic and neutral conditions. By contrast, no LLPS occurred in the GL/AS system, as shown in Fig. S2. In general, particles with low O:C are more prone to undergo LLPS. This observation is consistent with the findings of Song et al. (2012) who reported that LLPS was never observed when O:C > 0.80 and always observed when O:C < 0.56.

As shown in Fig. 2 and Table S2, for most spectra, WGMs remained after LLPS occurred for droplets of 3-MGA/AS. This phenomenon indicated that the droplets undergo LLPS with a core-shell morphology in most conditions, which is consistent with the prediction of Gorkowski et al. (2020). Meanwhile, morphology of phase-separated droplets containing either HEXT or HEXD were also core-shell shape mostly, as depicted in ~~Figure S3/S4~~ and Table S3/S4. It is attributed to the lower interfacial tension observed at higher O:C, leading to higher possibility condition for forming core-shell shaped droplets (Gorkowski et al., 2020). These findings support the idea that the O:C plays a crucial role in determining the morphology of phase-separated particles in organic/inorganic mixed aerosols.



335
 336 **Figure 4.** Van Krevelen Diagram for the mixed organic/AS particles: Solid symbols indicate that LLPS was observed, while
 337 hollow symbols indicate that LLPS was not observed. Solid triangles represent dicarboxylic acids (DOA, including malonic
 338 acid, malic acid, maleic acid, glutaric acid and diethylmalonic acid), sugars (levoglucosan), esters (including diethyl sebacate,
 339 suberic acid monomethyl ester and poly diacrylate), alcohols (including 2,5 hexanediol, propylene glycol and 1,2,6-
 340 hexanetriol), PEG (including PEG200 and PEG300) obtained from You et al. (2013), and AS PEG400 obtained from O'Brien
 341 et al. (2015).

342 4 Conclusion

343 The aim of this study was to investigate the effect of pH and O:C on phase transition behavior of levitated particles using the
 344 AOT. Our results show that across aerosol pH in atmospheric condition, the presence of sulfuric acid inhibited the LLPS of
 345 aerosol droplets that contained organics (3-MGA, HEXT, HEXD) and AS. Additionally, the MRHs were found to be higher
 346 than the SRHs. The O:C of phase-separating systems is 0.67, 0.50, 0.33, and by contrast, LLPS of the high O:C system (GL,
 347 O:C=1.00) did not occur. Meanwhile, the morphology of levitated aerosol particles was studied and we found that 38-42
 348 of 40-46 droplets that underwent LLPS for a core-shell structure. The SRH of all experimental systems ranged from ~70% to
 349 90%. In certain cases, as the RH decreased, the droplet morphology changed from core-shell to partially engulfed, similar to
 350 the findings reported by Kucinski et al. (2020). However, as the RH further decreased, the droplet particle size became smaller
 351 than 6 μm , making it impossible to capture them using AOT. Consequently, in most instances, we were unable to observe the
 352 droplet morphology at RH levels below 70%. The results presented here provide new insights into the behavior of different

353 types of aerosol droplets, and the findings have important implications for our understanding of physical and chemical
354 processes that occur in the atmosphere. It is anticipated that future studies will be carried out to examine the OIR-dependent
355 phase separation in real acidified ambient aerosols. Such research will provide insights into the morphological characteristics
356 of real aerosols and the ways in which these characteristics influence important properties such as hygroscopicity and
357 homogenous chemistry. Such information will be helpful in furthering our understanding of the impacts of ambient aerosols
358 on the environment and human health.

359
360 Additionally, in-situ measurement or pH estimation methods, such as the real-time AOT analysis in microdroplets reported
361 by Boyer et al. (2020) could be combined with SRH measurements for a more accurate and comprehensive analysis.
362 Furthermore, our study used a surrogate for SOA instead of in situ measurements of real SOA, which can be addressed in
363 future work using SOA generated from a smog chamber or real SOA precursors and oxidized species.

364
365 **Data availability.** The data used in this paper can be obtained from the corresponding author upon request.

366 **Author contributions.** YC built the instrument, performed the experiments, analyzed the data, plotted the figures, and wrote
367 the original draft. XP conceptualized the study, contributed to instrumentation, data analysis, discussion, and reviewed the
368 manuscript. HL and CX contributed to the instrumentation and discussion. YM contributed to the experiments and discussion.
369 ZX, FZ contributed to the discussion and manuscript review. TCP contributed to data analysis and manuscript review. ZW
370 administrated the project, conceptualized the study, reviewed the manuscript, and contributed to funding acquisition.

371 **Competing interests.** The contact author has declared that none of the authors has any competing interests.

372 **Disclaimer.** Publisher's note: Copernicus Publications remains neutral with regard to jurisdictional claims in published maps
373 and institutional affiliations.

374 **Financial support.** This research has been supported by the National Natural Science Foundation of China (grant nos.
375 91844301, 42005087, and 42005086), Key Research and Development Program of Zhejiang Province (grant nos. 2021C03165,
376 2022C03084), and the Fundamental Research Funds for the Central Universities (grant no. 2018QNA6008).

377 **References**

- 378 [Angle, K. J., Crocker, D. R., Simpson, R. M. C., Mayer, K. J., Garofalo, L. A., Moore, A. N., Mora Garcia, S. L., Or, V. W.,](#)
379 [Srinivasan, S., Farhan, M., Sauer, J. S., Lee, C., Pothier, M. A., Farmer, D. K., Martz, T. R., Bertram, T. H., Cappa, C. D.,](#)
380 [Prather, K. A., and Grassian, V. H.: Acidity across the interface from the ocean surface to sea spray aerosol, Proc. Natl. Acad.](#)
381 [Sci. U.S.A., 118, e2018397118, <https://doi.org/10.1073/pnas.2018397118>, 2021.](#)
382 [Bertram, A. K., Martin, S. T., Hanna, S. J., Smith, M. L., Bodsworth, A., Chen, Q., Kuwata, M., Liu, A., You, Y., and Zorn, S. R.:](#)
383 [Predicting the relative humidities of liquid-liquid phase separation, efflorescence, and deliquescence of mixed particles of](#)
384 [ammonium sulfate, organic material, and water using the organic-to-sulfate mass ratio of the particle and the oxygen-to-carbon](#)
385 [elemental ratio of the organic component, Atmos. Chem. Phys., 11, 10995-11006, <https://doi.org/10.5194/acp-11-10995-2011>,](#)
386 [2011.](#)

387 Boyer, H. C., Gorkowski, K., and Sullivan, R. C.: In situ pH measurements of individual levitated microdroplets using aerosol
388 optical tweezers, *Anal. Chem.*, 92, 1089-1096, <https://doi.org/10.1021/acs.analchem.9b04152>, 2020.

389 Canagaratna, M. R., Jimenez, J. L., Kroll, J. H., Chen, Q., Kessler, S. H., Massoli, P., Hildebrandt Ruiz, L., Fortner, E., Williams,
390 L. R., Wilson, K. R., Surratt, J. D., Donahue, N. M., Jayne, J. T., and Worsnop, D. R.: Elemental ratio measurements of organic
391 compounds using aerosol mass spectrometry: characterization, improved calibration, and implications, *Atmos. Chem. Phys.*,
392 15, 253-272, <https://doi.org/10.5194/acp-15-253-2015>, 2015.

393 Ciobanu, V. G.; Marcolli, C.; Krieger, U. K.; Weers, U.; Peter, T. **Liquid-Liquid Phase Separation in Mixed Organic/Inorganic**
394 **Aerosol Particles.** *J. Phys. Chem. A* 2009, 113 (41), 10966–10978.

395 Coddens, E. M., Angle, K. J., and Grassian, V. H.: Titration of aerosol pH through droplet coalescence, *J. Phys. Chem. Lett.*, 10,
396 4476-4483, <https://doi.org/10.1021/acs.jpcllett.9b00757>, 2019. Corral Arroyo, P., David, G., Alpert, P. A., Parmentier, E. A.,
397 Ammann, M., and Signorell, R.: Amplification of light within aerosol particles accelerates in-particle photochemistry, *Science*,
398 376, 293-296, <https://doi.org/10.1126/science.abm7915>, 2022.

399 Cosman, L. M., Knopf, D. A., and Bertram, A. K.: N₂O₅ reactive uptake on aqueous sulfuric acid solutions coated with branched
400 and straight-chain insoluble organic surfactants, *J. Phys. Chem. A*, 112, 2386, <https://doi.org/10.1021/jp710685r>, 2008.

401 Craig, R. L., Peterson, P. K., Nandy, L., Lei, Z., Hossain, M. A., Camarena, S., Dodson, R. A., Cook, R. D., Dutcher, C. S., and
402 Ault, A. P.: Direct Determination of Aerosol pH: Size-resolved measurements of submicrometer and supermicrometer aqueous
403 particles, *Anal. Chem.*, 90, 11232-11239, <https://doi.org/10.1021/acs.analchem.8b00586>, 2018.

404 Cui, X., Tang, M., Wang, M., and Zhu, T.: Water as a probe for pH measurement in individual particles using micro-Raman
405 spectroscopy, *Anal. Chim. Acta.*, 1186, 339089, <https://doi.org/10.1016/j.aca.2021.339089>, 2021.

406 Fang, T., Guo, H., Zeng, L., Verma, V., Nenes, A., and Weber, R. J.: Highly acidic ambient particles, soluble metals, and oxidative
407 potential: a link between sulfate and aerosol toxicity, *Environ. Sci. Technol.*, 51, 2611-2620,
408 <https://doi.org/10.1021/acs.est.6b06151>, 2017.

409 Freedman, M. A., Hasenkopf, C. A., Beaver, M. R., and Tolbert, M. A.: Optical properties of internally mixed aerosol particles
410 composed of dicarboxylic acids and ammonium sulfate, *J. Phys. Chem. A*, 113, 13584-13592,
411 <https://doi.org/10.1021/jp906240y>, 2009.

412 **Freedman, M. A.: Phase separation in organic aerosol, *Chem. Soc. Rev.*, 46, 7694-7705, <http://doi.org/10.1039/C6CS00783J>, 2017.**

413 Freedman, M. A.: Liquid-liquid phase separation in supermicrometer and submicrometer aerosol particles, *Acc. Chem. Res.*, 53,
414 1102-1110, <https://doi.org/10.1021/acs.accounts.0c00093>, 2020.

415 Gong, Z. Y., Pan, Y. L., Videen, G., and Wang, C. J.: Optical trapping and manipulation of single particles in air: principles,
416 technical details, and applications, *J. Quant. Spectrosc. Ra.*, 214, 94-119, <https://doi.org/10.1016/j.jqsrt.2018.04.027>, 2018.

417 Gorkowski, K., Donahue, N. M., and Sullivan, R. C.: Emulsified and liquid-liquid phase-separated states of alpha-pinene secondary
418 organic aerosol determined using aerosol optical tweezers, *Environ. Sci. Technol.*, 51, 12154-12163,
419 <https://doi.org/10.1021/acs.est.7b03250>, 2017.

420 Gorkowski, K., Donahue, N. M., and Sullivan, R. C.: Aerosol optical tweezers constrain the morphology evolution of liquid-liquid
421 phase-separated atmospheric particles, *Chem*, 6, 204-220, <https://doi.org/10.1016/j.chempr.2019.10.018>, 2020.

422 Guo, H., Liu, J., Froyd, K. D., Roberts, J. M., Veres, P. R., Hayes, P. L., Jimenez, J. L., Nenes, A., and Weber, R. J.: Fine particle
423 pH and gas-particle phase partitioning of inorganic species in Pasadena, California, during the 2010 CalNex campaign, *Atmos.*
424 *Chem. Phys.*, 17, 5703-5719, <https://doi.org/10.5194/acp-17-5703-2017>, 2017.

425 Kucinski, T. M., Dawson, J. N., and Freedman, M. A.: Size-Dependent Liquid-Liquid Phase Separation in Atmospherically
426 Relevant Complex Systems, *J. Phys. Chem. Lett.*, 10, 6915-6920, <https://doi.org/10.1021/acs.jpcllett.9b02532>, 2019.

427 **Kucinski, T. M., Ott, E.-J. E., and Freedman, M. A.: Flash Freeze Flow Tube to Vitrify Aerosol Particles at Fixed Relative Humidity**
428 **Values, *Anal. Chem.*, 92, 5207-5213, <https://doi.org/10.1021/acs.analchem.9b05757>, 2020.**

429 Kucinski, T. M., Ott, E. E., and Freedman, M. A.: Dynamics of liquid-liquid phase separation in submicrometer aerosol, *J. Phys.*
430 *Chem. A.*, 125, 4446-4453, <https://doi.org/10.1021/acs.jpca.1c01985>, 2021.

431 Lam, H. K., Xu, R., Choczynski, J., Davies, J. F., Ham, D., Song, M., Zuend, A., Li, W., Tse, Y. L. S., and Chan, M. N.: Effects of
432 liquid-liquid phase separation and relative humidity on the heterogeneous OH oxidation of inorganic-organic aerosols:
433 insights from methylglutaric acid and ammonium sulfate particles, *Atmos. Chem. Phys.*, 21, 2053-2066,
434 <https://doi.org/10.5194/acp-21-2053-2021>, 2021.

435 Li, M., Su, H., Zheng, G., Kuhn, U., Kim, N., Li, G., Ma, N., Pöschl, U., and Cheng, Y.: Aerosol pH and ion activities of HSO₄⁻
436 and SO₄²⁻ in supersaturated single droplets, *Environ. Sci. Technol.*, <https://doi.org/10.1021/acs.est.2e01378>, 2022.

437 Li, M., Kan, Y., Su, H., Pöschl, U., Parekh, S. H., Bonn, M., and Cheng, Y. F.: Spatial homogeneity of pH in aerosol microdroplets,
438 Chem, in press, <https://doi.org/10.1016/j.chempr.2023.02.019>, 2023.

439 Lin, H. B., Eversole, J. D., and Campillo, A. J.: Continuous-wave stimulated Raman scattering in microdroplets, P. Opt. Lett., 17,
440 828–830, <https://doi.org/10.1364/ol.17.000828>, 1992.

441 Liu, M., Huang, X., Song, Y., Tang, J., Cao, J., Zhang, X., Zhang, Q., Wang, S., Xu, T., Kang, L., Cai, X., Zhang, H., Yang, F.,
442 Wang, H., Yu, J. Z., Lau, A. K. H., He, L., Huang, X., Duan, L., Ding, A., Xue, L., Gao, J., Liu, B., and Zhu, T.: Ammonia
443 emission control in China would mitigate haze pollution and nitrogen deposition, but worsen acid rain, Proc. Natl. Acad. Sci.
444 U. S. A., 116, 7760–7765, <https://doi.org/10.1073/pnas.1814880116>, 2019. Losey, D. J., Parker, R. G., and Freedman, M. A.:
445 pH Dependence of Liquid–Liquid Phase Separation in Organic Aerosol, The journal of physical chemistry letters, 7, 3861–
446 3865, [10.1021/acs.jpcllett.6b01621](https://doi.org/10.1021/acs.jpcllett.6b01621), 2016.

447 Losey, D. J., Ott, E. J. E., and Freedman, M. A.: Effects of high acidity on phase transitions of an organic aerosol, J. Phys. Chem.
448 A, 122, 3819–3828, <https://doi.org/10.1021/acs.jpca.8b00399>, 2018.

449 Ma, S. S., Chen, Z., Pang, S. F., and Zhang, Y. H.: Observations on hygroscopic growth and phase transitions of mixed 1, 2, 6-
450 hexanetriol/(NH₄)₂SO₄ particles: investigation of the liquid–liquid phase separation (LLPS) dynamic process and mechanism
451 and secondary LLPS during the dehumidification, Atmos. Chem. Phys., 21, 9705–9717, [https://doi.org/10.5194/acp-21-9705-](https://doi.org/10.5194/acp-21-9705-2021)
452 2021, 2021.

453 Mahrt, F., Newman, E., Huang, Y., Ammann, M., and Bertram, A. K.: Phase behavior of hydrocarbon-like primary organic aerosol
454 and secondary organic aerosol proxies based on their elemental oxygen-to-carbon ratio, Environ. Sci. Technol., 55, 12202–
455 12214, <https://doi.org/10.1021/acs.est.1c02697>, 2021.

456 Mikhailov, E. F., Pöhlker, M. L., Reinmuth-Selzle, K., Vlasenko, S. S., Krüger, O. O., Fröhlich-Nowoisky, J., Pöhlker, C., Ivanova,
457 O. A., Kiselev, A. A., Kremper, L. A., and Pöschl, U.: Water uptake of subpollen aerosol particles: hygroscopic growth, cloud
458 condensation nuclei activation, and liquid–liquid phase separation, Atmos. Chem. Phys., 21, 6999–7022,
459 <https://doi.org/10.5194/acp-21-6999-2021>, 2021.

460 Mitchem, L., Buajarnern, J., Ward, A. D., and Reid, J. P.: A strategy for characterizing the mixing state of immiscible aerosol
461 components and the formation of multiphase aerosol particles through coagulation, J. Phys. Chem. B, 110, 13700–13703,
462 <https://doi.org/10.1021/jp062874z>, 2006.

463 O'Brien, R. E., Wang, B. B., Kelly, S. T., Lundt, N., You, Y., Bertram, A. K., Leone, S. R., Laskin, A., and Gilles, M. K.: Liquid-
464 liquid phase separation in aerosol particles: imaging at the nanometer scale, Environ. Sci. Technol., 49, 4995–5002,
465 <https://doi.org/10.1021/acs.est.5b00062>, 2015.

466 O'Haver, T. C.: A pragmatic introduction to signal processing with applications in scientific measurement, Kindle Direct Publishing,
467 ISBN: 9798611266687, 2022.

468 Ohno, P. E., Qin, Y., Ye, J., Wang, J., Bertram, A. K., and Martin, S. T.: Fluorescence aerosol flow tube spectroscopy to detect
469 liquid–liquid phase separation, ACS Earth Space Chem., 5, 1223–1232, <http://doi.org/10.1021/acsearthspacechem.1c00061>,
470 2021.

471 Ott, E.-J. E., Tackman, E. C., and Freedman, M. A.: Effects of Sucrose on Phase Transitions of Organic/Inorganic Aerosols, ACS
472 Earth Space Chem., 4, 591–601, <http://doi.org/10.1021/acsearthspacechem.0c00006>, 2020.

473 Petters, M. D. and Kreidenweis, S. M.: A single parameter representation of hygroscopic growth and cloud condensation nucleus
474 activity, Atmos. Chem. Phys., 7, 1961–1971, <https://doi.org/10.5194/acp-7-1961-2007>, 2007.

475 Preston, T. C. and Reid, J. P.: Accurate and efficient determination of the radius, refractive index, and dispersion of weakly
476 absorbing spherical particle using whispering gallery modes, J. Opt. Soc. Am. B, 30, 2113–2122,
477 <https://doi.org/10.1364/JOSAB.30.002113>, 2013.

478 Preston, T. C. and Reid, J. P.: Determining the size and refractive index of microspheres using the mode assignments from Mie
479 resonances, J. Opt. Soc. Am. A, 32, 2210–2217, <https://doi.org/10.1364/JOSAA.32.002210>, 2015.

480 Pye, H. O. T., Nenes, A., Alexander, B., Ault, A. P., Barth, M. C., Clegg, S. L., Collett, J. L., Jr., Fahey, K. M., Hennigan, C. J.,
481 Herrmann, H., Kanakidou, M., Kelly, J. T., Ku, I. T., McNeill, V. F., Riemer, N., Schaefer, T., Shi, G., Tilgner, A., Walker, J.
482 T., Wang, T., Weber, R., Xing, J., Zaveri, R. A., and Zuend, A.: The acidity of atmospheric particles and clouds, Atmos. Chem.
483 Phys., 20, 4809–4888, <https://doi.org/10.5194/acp-20-4809-2020>, 2020.

484 Rafferty, A., Vennes, B., Bain, A., and Preston, T. C.: Optical trapping and light scattering in atmospheric aerosol science, Phys.
485 Chem. Chem. Phys., 25, 7066–7089, <https://doi.org/10.1039/d2cp05301b>, 2023.

486 Redding, B., Schwab, M. J., and Pan, Y. L.: Raman spectroscopy of optically trapped single biological micro-particles, *Sensors*, 15,
487 19021-19046, <https://doi.org/10.3390/s150819021>, 2015.

488 Reid, J. P., Dennis-Smith, B. J., Kwamena, N. O. A., Miles, R. E. H., Hanford, K. L., and Homer, C. J.: The morphology of
489 aerosol particles consisting of hydrophobic and hydrophilic phases: hydrocarbons, alcohols and fatty acids as the hydrophobic
490 component, *Phys. Chem. Chem. Phys.*, 13, 15559-15572, <https://doi.org/10.1039/c1cp21510h>, 2011.

491 Rosenfeld, D., Sherwood, S., Wood, R., and Donner, L.: Climate effects of aerosol-cloud interactions, *Science*, 343, 379-380,
492 <https://doi.org/10.1126/science.1247490>, 2014.

493 Freedman, M. A., Hasenkopf, C. A., Beaver, M. R., and Tolbert, M. A.: Optical properties of internally mixed aerosol particles
494 composed of dicarboxylic acids and ammonium sulfate, *J. Phys. Chem. A*, 113, 13584-13592,
495 <https://doi.org/10.1021/jp906240y>, 2009.

496 Corral-Arroyo, P., David, G., Alpert, P. A., Parmentier, E. A., Ammann, M., and Signorini, R.: Amplification of light within aerosol
497 particles accelerates in-particle photochemistry, *Science*, 376, 293-296, <https://doi.org/10.1126/science.1247915>, 2022.

498 Cosman, L. M., Knopf, D. A., and Bertram, A. K.: N₂O₅ reactive uptake on aqueous sulfuric acid solutions coated with branched
499 and straight chain insoluble organic surfactants, *J. Phys. Chem. A*, 112, 2386, <https://doi.org/10.1021/jp710685r>, 2008.

500 Lam, H. K., Xu, R., Choczynski, J., Davies, J. F., Ham, D., Song, M., Zuend, A., Li, W., Tse, Y. L. S., and Chan, M. N.: Effects of
501 liquid-liquid phase separation and relative humidity on the heterogeneous OH oxidation of inorganic organic aerosols:
502 insights from methylglutaric acid and ammonium sulfate particles, *Atmos. Chem. Phys.*, 21, 2053-2066,
503 <https://doi.org/10.5194/acp-21-2053-2021>, 2021.

504 Peters, M. D. and Kreidenweis, S. M.: A single parameter representation of hygroscopic growth and cloud condensation nucleus
505 activity, *Atmos. Chem. Phys.*, 7, 1961-1971, <https://doi.org/10.5194/acp-7-1961-2007>, 2007.

506 Mikhailov, E. F., Pöhlker, M. L., Reinmuth Selzle, K., Vlasenko, S. S., Krüger, O. O., Fröhlich Nowojsky, J., Pöhlker, C., Ivanova,
507 O. A., Kiselev, A. A., Krempner, L. A., and Pöschl, U.: Water uptake of subpollen aerosol particles: hygroscopic growth, cloud
508 condensation nuclei activation, and liquid-liquid phase separation, *Atmos. Chem. Phys.*, 21, 6999-7022,
509 <https://doi.org/10.5194/acp-21-6999-2021>, 2021.

510 Gorkowski, K., Donahue, N. M., and Sullivan, R. C.: Aerosol optical tweezers constrain the morphology evolution of liquid-liquid
511 phase-separated atmospheric particles, *Chem*, 6, 204-220, <https://doi.org/10.1016/j.chempr.2019.10.018>, 2020.

512 Freedman, M. A.: Liquid-liquid phase separation in supermicrometer and submicrometer aerosol particles, *Acc. Chem. Res.*, 53,
513 1102-1110, <https://doi.org/10.1021/acs.accounts.0c00093>, 2020.

514 Gorkowski, K., Donahue, N. M., and Sullivan, R. C.: Emulsified and liquid-liquid phase-separated states of alpha-pinene secondary
515 organic aerosol determined using aerosol optical tweezers, *Environ. Sci. Technol.*, 51, 12154-12163,
516 <https://doi.org/10.1021/acs.est.7b03250>, 2017.

517 Song, M., Marcolli, C., Krieger, U. K., Zuend, A., and Peter, T.: Liquid-liquid phase separation in aerosol particles: dependence on
518 O:C, organic functionalities, and compositional complexity, *Geophys. Res. Lett.*, 39, L19801,
519 <https://doi.org/10.1029/2012GL052807>, 2012.

520 Song, M. J., Marcolli, C., Krieger, U. K., Lienhard, D. M., and Peter, T.: Morphologies of mixed organic/inorganic/aqueous aerosol
521 droplets, *Faraday Discuss.*, 165, 289-316, <https://doi.org/10.1039/c3fd00049d>, 2013.

522 Song, S., Gao, M., Xu, W., Shao, J., Shi, G., Wang, S., Wang, Y., Sun, Y., and McElroy, M. B.: Fine particle pH for Beijing winter
523 haze as inferred from different thermodynamic equilibrium models, *Atmos. Chem. Phys.*, 18, 7423-7438,
524 <https://doi.org/10.5194/acp-18-7423-2018>, 2018.

525 Kucinski, T. M., Ott, E. E., and Freedman, M. A.: Dynamics of liquid-liquid phase separation in submicrometer aerosol, *J. Phys.*
526 *Chem. A*, 125, 4446-4453, <https://doi.org/10.1021/acs.jpca.1c01985>, 2021.

527 Stewart, D. J., Cai, C., Naylor, J., Preston, T. C., Reid, J. P., Krieger, U. K., Marcolli, C., and Zhang, Y. H.: Liquid-liquid phase
528 separation in mixed organic/inorganic single aqueous aerosol droplets, *J. Phys. Chem. A*, 119, 4177-4190,
529 <https://doi.org/10.1021/acs.jpca.5b01658>, 2015.

530 Sullivan, R. C., Boyer-Chelmo, H., Gorkowski, K., and Beydoun, H.: Aerosol Optical Tweezers Elucidate the Chemistry, Acidity,
531 Phase Separations, and Morphology of Atmospheric Microdroplets, *Acc. Chem. Res.*, 11, 2498-2509,
532 <https://doi.org/10.1021/acs.accounts.0c00407>, 2020.

533 Tilgner, A., Schaefer, T., Alexander, B., Barth, M., Collett, J. L., Fahey, K. M., Nenes, A., Pye, H. O. T., Herrmann, H., and McNeill,
534 V. F.: Acidity and the multiphase chemistry of atmospheric aqueous particles and clouds, *Atmos. Chem. Phys.*, 21, 13483-
535 13536, <https://doi.org/10.5194/acp-21-13483-2021>, 2021.

536 Tong, Y. K., Meng, X. X. Y., Zhou, B., Sun, R., Wu, Z. J., Hu, M., and Ye, A. P.: Detecting the pH-dependent liquid-liquid phase
537 separation of single levitated aerosol microdroplets via laser tweezers-Raman spectroscopy, *Front. Phys.*, 10,
538 <https://doi.org/10.3389/fphy.2022.969921>, 2022.

539 Wade, L. G. and Simek, J. W.: Acidity of alcohols and phenols, in: *Organic Chemistry*, <https://chem.libretexts.org/@go/page/45234>,
540 2020.

541 Wang, M., Zheng, N., Zhao, D., Shang, J., and Zhu, T.: Using micro-Raman spectroscopy to investigate chemical composition,
542 mixing states, and heterogeneous reactions of individual atmospheric particles, *Environ. Sci. Technol.*, 55, 10243-10254,
543 <https://doi.org/10.1021/acs.est.1c01242>, 2021.

544 Pye, H. O. T., Nenes, A., Alexander, B., Ault, A. P., Barth, M. C., Clegg, S. L., Collett, J. L., Jr., Fahey, K. M., Hennigan, C.
545 J., Herrmann, H., Kanakidou, M., Kelly, J. T., Ku, J. T., McNeill, V. F., Riemer, N., Schaefer, T., Shi, G., Tilgner, A., Walker,
546 J. T., Wang, T., Weber, R., Xing, J., Zaveri, R. A., and Zuend, A.: The acidity of atmospheric particles and clouds, *Atmos.*
547 *Chem. Phys.*, 20, 4809-4888, <https://doi.org/10.5194/acp-20-4809-2020>, 2020.

548 Angle, K. J., Crocker, D. R., Simpson, R. M. C., Mayer, K. J., Garofalo, L. A., Moore, A. N., Mora Garcia, S. L., Or, V. W.,
549 Srinivasan, S., Farhan, M., Sauer, J. S., Lee, C., Pothier, M. A., Farmer, D. K., Martz, T. R., Bertram, T. H., Cappa, C. D.,
550 Prather, K. A., and Grassian, V. H.: Acidity across the interface from the ocean surface to sea spray aerosol, *Proc. Natl. Acad.*
551 *Sci. U.S.A.*, 118, e2018397118, <https://doi.org/10.1073/pnas.2018397118>, 2021.

552 Weber, R. J., Guo, H. Y., Russell, A. G., and Nenes, A.: High aerosol acidity despite declining atmospheric sulfate concentrations
553 over the past 15 years, *Nat. Geosci.*, 9, 282-285, <https://doi.org/10.1038/ngeo2665>, 2016.

554 Tilgner, A., Schaefer, T., Alexander, B., Barth, M., Collett, J. L., Fahey, K. M., Nenes, A., Pye, H. O. T., Herrmann, H., and
555 McNeill, V. F.: Acidity and the multiphase chemistry of atmospheric aqueous particles and clouds, *Atmos. Chem. Phys.*, 21,
556 13483-13536, <https://doi.org/10.5194/acp-21-13483-2021>, 2021.

557 Zheng, G., Su, H., Wang, S., Andreae, M., Pöschl, U., and Cheng, Y.: Multiphase buffer theory explains contrasts in
558 atmospheric aerosol acidity, *Science*, 369, 1374-1377, <https://doi.org/10.1126/science.aba3719>, 2020.

559 Fang, T., Guo, H., Zeng, L., Verma, V., Nenes, A., and Weber, R. J.: Highly acidic ambient particles, soluble metals, and
560 oxidative potential: a link between sulfate and aerosol toxicity, *Environ. Sci. Technol.*, 51, 2611-2620,
561 <https://doi.org/10.1021/acs.est.6b06151>, 2017.

562 Young, A. H., Keene, W. C., Pszenny, A. A. P., Sander, R., Thornton, J. A., Riedel, T. P., and Maben, J. R.: Phase partitioning
563 of soluble trace gases with size-resolved aerosols in near-surface continental air over northern Colorado, USA, during winter,
564 *J. Geophys. Res.: Atmospheres*, 118, 9414-9427, <https://doi.org/10.1002/jgrd.50655>, 2013.

565 Guo, H., Liu, J., Froyd, K. D., Roberts, J. M., Veros, P. R., Hayes, P. L., Jimenez, J. L., Nenes, A., and Weber, R. J.: Fine
566 particle pH and gas-particle phase partitioning of inorganic species in Pasadena, California, during the 2010 CalNex campaign,
567 *Atmos. Chem. Phys.*, 17, 5703-5719, <https://doi.org/10.5194/acp-17-5703-2017>, 2017.

568 Losey, D. J., Ott, E. J. E., and Freedman, M. A.: Effects of high acidity on phase transitions of an organic aerosol, *J. Phys.*
569 *Chem. A*, 122, 3819-3828, <https://doi.org/10.1021/acs.jpca.8b00399>, 2018.

570 Tong, Y. K., Meng, X. X. Y., Zhou, B., Sun, R., Wu, Z. J., Hu, M., and Ye, A. P.: Detecting the pH-dependent liquid-liquid
571 phase separation of single levitated aerosol microdroplets via laser tweezers Raman spectroscopy, *Front. Phys.*, 10,
572 <https://doi.org/10.3389/fphy.2022.969921>, 2022.

573 Wang, M., Zheng, N., Zhao, D., Shang, J., and Zhu, T.: Using micro-Raman spectroscopy to investigate chemical composition,
574 mixing states, and heterogeneous reactions of individual atmospheric particles, *Environ. Sci. Technol.*, 55, 10243-10254,
575 <https://doi.org/10.1021/acs.est.1c01242>, 2021.

576 Cui, X., Tang, M., Wang, M., and Zhu, T.: Water as a probe for pH measurement in individual particles using micro-Raman
577 spectroscopy, *Anal. Chim. Acta.*, 1186, 339089, <https://doi.org/10.1016/j.aca.2021.339089>, 2021.

578 Redding, B., Schwab, M. J., and Pan, Y. L.: Raman spectroscopy of optically trapped single biological micro-particles, *Sensors*, 15,
579 19021-19046, <https://doi.org/10.3390/s150819021>, 2015.

580 Gong, Z. Y., Pan, Y. L., Videon, G., and Wang, C. J.: Optical trapping and manipulation of single particles in air: principles,
581 technical details, and applications, *J. Quant. Spectrosc. Ra.*, 214, 94-119, <https://doi.org/10.1016/j.jqsrt.2018.04.027>, 2018.

582 Rafferty, A., Vennes, B., Bain, A., and Preston, T. C.: Optical trapping and light scattering in atmospheric aerosol science, *Phys.*
583 *Chem. Chem. Phys.*, 25, 7066-7089, <https://doi.org/10.1039/d2cp05301b>, 2023.

584 Canagaratna, M. R., Jimenez, J. L., Kroll, J. H., Chen, Q., Kessler, S. H., Massoli, P., Hildebrandt Ruiz, L., Fortner, E., Williams,
585 L. R., Wilson, K. R., Surratt, J. D., Donahue, N. M., Jayne, J. T., and Worsnop, D. R.: Elemental ratio measurements of organic

586 compounds using aerosol mass spectrometry: characterization, improved calibration, and implications, *Atmos. Chem. Phys.*,
587 15, 253–272, <https://doi.org/10.5194/acp-15-253-2015>, 2015.

588 Mahrt, F., Newman, E., Huang, Y., Ammann, M., and Bertram, A. K.: Phase behavior of hydrocarbon-like primary organic aerosol
589 and secondary organic aerosol proxies based on their elemental oxygen-to-carbon ratio, *Environ. Sci. Technol.*, 55, 12202–
590 12214, <https://doi.org/10.1021/acs.est.1c02697>, 2021.

591 Lin, H. B., Eversole, J. D., and Campillo, A. J.: Continuous-wave stimulated Raman scattering in microdroplets, *P. Opt. Lett.*, 17,
592 828–830, <https://doi.org/10.1364/ol.17.000828>, 1992.

593 Mitchem, L., Buajarern, J., Ward, A. D., and Reid, J. P.: A strategy for characterizing the mixing state of immiscible aerosol
594 components and the formation of multiphase aerosol particles through coagulation, *J. Phys. Chem. B*, 110, 13700–13703,
595 <https://doi.org/10.1021/jp062874z>, 2006.

596 Reid, J. P., Dennis Smither, B. J., Kwamona, N. O. A., Miles, R. E. H., Hanford, K. L., and Homer, C. J.: The morphology of
597 aerosol particles consisting of hydrophobic and hydrophilic phases: hydrocarbons, alcohols and fatty acids as the hydrophobic
598 component, *Phys. Chem. Chem. Phys.*, 13, 15559–15572, <https://doi.org/10.1039/c1cp21510h>, 2011.

599 Sullivan, R. C., Boyer-Chelmo, H., Gorkowski, K., and Beydoun, H.: Aerosol Optical Tweezers Elucidate the Chemistry, Acidity,
600 Phase Separations, and Morphology of Atmospheric Microdroplets, *Acc. Chem. Res.*, 11, 2498–2509,
601 <https://doi.org/10.1021/acs.accounts.0c00407>, 2020.

602 O'Haver, T. C.: A pragmatic introduction to signal processing with applications in scientific measurement, Kindle Direct Publishing,
603 ISBN: 9798611266687, 2022.

604 Preston, T. C. and Reid, J. P.: Accurate and efficient determination of the radius, refractive index, and dispersion of weakly
605 absorbing spherical particle using whispering gallery modes, *J. Opt. Soc. Am. B*, 30, 2113–2122,
606 <https://doi.org/10.1364/JOSAB.30.002113>, 2013.

607 Preston, T. C. and Reid, J. P.: Determining the size and refractive index of microspheres using the mode assignments from Mie
608 resonances, *J. Opt. Soc. Am. A*, 32, 2210–2217, <https://doi.org/10.1364/JOSAA.32.002210>, 2015.

609 Bertram, A. K., Martin, S. T., Hanna, S. J., Smith, M. L., Bodsworth, A., Chen, Q., Kuwata, M., Liu, A., You, Y., and Zorn, S. R.:
610 Predicting the relative humidities of liquid-liquid phase separation, efflorescence, and deliquescence of mixed particles of
611 ammonium sulfate, organic material, and water using the organic-to-sulfate mass ratio of the particle and the oxygen-to-carbon
612 elemental ratio of the organic component, *Atmos. Chem. Phys.*, 11, 10995–11006, <https://doi.org/10.5194/acp-11-10995-2011>,
613 2011.

614 Boyer, H. C., Gorkowski, K., and Sullivan, R. C.: In situ pH measurements of individual levitated microdroplets using aerosol
615 optical tweezers, *Anal. Chem.*, 92, 1089–1096, <https://doi.org/10.1021/acs.analchem.9b04152>, 2020.

616 Coddens, E. M., Angle, K. J., and Grassian, V. H.: Titration of aerosol pH through droplet coalescence, *J. Phys. Chem. Lett.*, 10,
617 4476–4483, <https://doi.org/10.1021/acs.jpclett.9b00757>, 2019.

618 Craig, R. L., Peterson, P. K., Nandy, L., Lei, Z., Hossain, M. A., Camarena, S., Dodson, R. A., Cook, R. D., Dutcher, C. S., and
619 Ault, A. P.: Direct Determination of Aerosol pH: Size-resolved measurements of submicrometer and supermicrometer aqueous
620 particles, *Anal. Chem.*, 90, 11232–11239, <https://doi.org/10.1021/acs.analchem.8b00586>, 2018.

621 Kucinski, T. M., Dawson, J. N., and Freedman, M. A.: Size-Dependent Liquid-Liquid Phase Separation in Atmospherically
622 Relevant Complex Systems, *J. Phys. Chem. Lett.*, 10, 6915–6920, <https://doi.org/10.1021/acs.jpclett.9b02532>, 2019.

623 Li, M., Kan, Y., Su, H., Pöschl, U., Parekh, S. H., Bonn, M., and Cheng, Y. F.: Spatial homogeneity of pH in aerosol microdroplets,
624 *Chem*, in press, <https://doi.org/10.1016/j.chempr.2023.02.019>, 2023.

625 Li, M., Su, H., Zheng, G., Kuhn, U., Kim, N., Li, G., Ma, N., Pöschl, U., and Cheng, Y.: Aerosol pH and ion activities of HSO_4^-
626 and SO_4^{2-} in supersaturated single droplets, *Environ. Sci. Technol.*, <https://doi.org/10.1021/acs.est.2c01378>, 2022.

627 Liu, M., Huang, X., Song, Y., Tang, J., Cao, J., Zhang, X., Zhang, Q., Wang, S., Xu, T., Kang, L., Cai, X., Zhang, H., Yang, F.,
628 Wang, H., Yu, J. Z., Lau, A. K. H., He, L., Huang, X., Duan, L., Ding, A., Xue, L., Gao, J., Liu, B., and Zhu, T.: Ammonia
629 emission control in China would mitigate haze pollution and nitrogen deposition, but worsen acid rain, *Proc. Natl. Acad. Sci.*
630 *U. S. A.*, 116, 7760–7765, <https://doi.org/10.1073/pnas.1814880116>, 2019.

631 Ma, S. S., Chen, Z., Pang, S. F., and Zhang, Y. H.: Observations on hygroscopic growth and phase transitions of mixed 1, 2, 6-
632 hexanetriol/(NH_4)₂ SO_4 particles: investigation of the liquid-liquid phase separation (LLPS) dynamic process and mechanism
633 and secondary LLPS during the dehumidification, *Atmos. Chem. Phys.*, 21, 9705–9717, [https://doi.org/10.5194/acp-21-9705-](https://doi.org/10.5194/acp-21-9705-2021)
634 [2021](https://doi.org/10.5194/acp-21-9705-2021), 2021.

635 ~~O'Brien, R. E., Wang, B. B., Kelly, S. T., Lundt, N., You, Y., Bertram, A. K., Leone, S. R., Laskin, A., and Gilles, M. K.: Liquid-~~
636 ~~liquid phase separation in aerosol particles: imaging at the nanometer scale, Environ. Sci. Technol., 49, 4995-5002,~~
637 ~~<https://doi.org/10.1021/aes.est.5b00062>, 2015.~~
638 ~~Song, M. J., Marcolli, C., Krieger, U. K., Lienhard, D. M., and Peter, T.: Morphologies of mixed organic/inorganic/aqueous aerosol~~
639 ~~droplets, Faraday Discuss., 165, 289-316, <https://doi.org/10.1039/c3fd00049d>, 2013.~~
640 ~~Song, S., Gao, M., Xu, W., Shao, J., Shi, G., Wang, S., Wang, Y., Sun, Y., and McElroy, M. B.: Fine particle pH for Beijing winter~~
641 ~~haze as inferred from different thermodynamic equilibrium models, Atmos. Chem. Phys., 18, 7423-7438,~~
642 ~~<https://doi.org/10.5194/acp-18-7423-2018>, 2018.~~
643 ~~Wade, L. G. and Simcik, J. W.: Acidity of alcohols and phenols, in: Organic Chemistry, <https://chem.libretexts.org/@go/page/45234>,~~
644 ~~2020.~~
645 You, Y., Renbaum-Wolff, L., and Bertram, A. K.: Liquid-liquid phase separation in particles containing organics mixed with
646 ammonium sulfate, ammonium bisulfate, ammonium nitrate or sodium chloride, Atmos. Chem. Phys., 13, 11723-11734,
647 <https://doi.org/10.5194/acp-13-11723-2013>, 2013.
648 [You, Y., Smith, M. L., Song, M., Martin, S. T., Bertram, A. K.: Liquid-liquid phase separation in atmospherically relevant particles](#)
649 [consisting of organic species and inorganic salts, Int. Rev. Phys. Chem., 33 \(1\), 43-77,](#)
650 <http://doi.org/10.1080/0144235X.2014.890786>, 2014.
651 [Young, A. H., Keene, W. C., Pszenny, A. A. P., Sander, R., Thornton, J. A., Riedel, T. P., and Maben, J. R.: Phase partitioning of](#)
652 [soluble trace gases with size-resolved aerosols in near-surface continental air over northern Colorado, USA, during winter, J.](#)
653 [Geophys. Res.: Atmospheres, 118, 9414-9427, <https://doi.org/10.1002/jgrd.50655>, 2013.](#)
654 [Zheng, G., Su, H., Wang, S., Andreae, M., Pöschl, U., and Cheng, Y.: Multiphase buffer theory explains contrasts in atmospheric](#)
655 [aerosol acidity, Science, 369, 1374-1377, <https://doi.org/10.1126/science.aba3719>, 2020.](#)
656 [Zhou, Q., Pang, S.-F., Wang, Y., Ma, J.-B., and Zhang, Y.-H.: Confocal Raman studies of the evolution of the physical state](#)
657 [of mixed phthalic acid/ammonium sulfate aerosol droplets and the effect of substrates, J. Phys. Chem. B, 118, 6198-6205,](#)
658 <https://doi.org/10.1021/jp5004598>, 2014.